

Spin-charge-orbital ordering in hollandite-type manganites studied by model Hartree-Fock calculation

Makoto Fukuzawa,¹ Daiki Ootsuki,¹ and Takashi Mizokawa^{2,1}

¹*Department of Physics, University of Tokyo, 5-1-5 Kashiwanoha, Kashiwa, Chiba 277-8561, Japan*

²*Department of Complexity Science and Engineering, University of Tokyo, 5-1-5 Kashiwanoha, Kashiwa, Chiba 277-8561, Japan*

(Dated: October 11, 2018)

We investigate spin-charge-orbital ordering in a $\text{Mn}^{3+}/\text{Mn}^{4+}$ mixed valence state on a hollandite-type lattice using unrestricted Hartree-Fock calculation on a multi-band Mn $3d$ -O $2p$ lattice model. The calculations show that the Mn^{3+} - Mn^{4+} double exchange interaction, the Mn^{3+} - Mn^{3+} and Mn^{4+} - Mn^{4+} superexchange interactions are ferromagnetic and play important roles to stabilize the charge and orbital ordering pattern. The most stable charge and orbital ordering pattern is consistent with the $1 \times 1 \times 1$ orthorhombic or monoclinic structure of $\text{K}_{1.6}\text{Mn}_8\text{O}_{16}$.

PACS numbers: 71.30.+h, 71.28.+d, 75.25.Dk

I. INTRODUCTION

Various transition-metal oxides are known to show structural phase transitions which are accompanied by electronic transitions such as spin, charge, or orbital orderings [1, 2]. Such phase transitions in perovskite-type transition-metal oxides including $\text{La}_{1-x}\text{Ca}_x\text{MnO}_3$ have been studied experimentally and theoretically, and the relationship between the structural transition and the charge-orbital ordering of transition-metal d electrons has been revealed [3]. In the perovskite-type oxides, MO_6 (M = transition metal) octahedra share their corners and the electronic interaction between the neighboring sites is dominated by the M -O- M bond. On the other hand, transition-metal oxides with edge-sharing MO_6 octahedra including spinel-type Fe_3O_4 [4] and rutile-type VO_2 [5], the direct M - M bond also plays important role and often induces M - M dimer formation.

Recently, novel structural transitions have been discovered in hollandite-type transition-metal oxides such as $\text{K}_2\text{V}_8\text{O}_{16}$ [6] and $\text{K}_2\text{Cr}_8\text{O}_{16}$. [7] Since, in the hollandite-type structure, MO_6 octahedra share the corners and the edges, both the M - M and M -O- M bonds contribute to generate spin-charge-orbital orderings. Therefore, the hollandite-type oxides have been inspiring efforts to develop new theoretical framework to describe possible mechanism of the structural transitions. For example, $\text{K}_2\text{V}_8\text{O}_{16}$ exhibits two step jumps of resistivity in the narrow temperature range around 170 K which correspond to two structural transitions from a high-temperature tetragonal structure to an intermediate-temperature tetragonal structure to a low-temperature monoclinic (almost orthorhombic) $\sqrt{2} \times \sqrt{2} \times 2$ structure. [6] Since the formal valence of the V site is +3.75 for $\text{K}_2\text{V}_8\text{O}_{16}$, it is expected that the metal-insulator transition and structural transitions are driven by charge ordering between V^{3+} and V^{4+} and the V^{4+} - V^{4+} dimer formation along the V-O double chain or the V-O ribbon. [8–12] On the other hand, the structural transition in $\text{K}_2\text{Cr}_8\text{O}_{16}$ is well described as a Peierls transition of the

itinerant Cr $3d$ t_{2g} electrons. [13]

Compared to $\text{K}_2\text{V}_8\text{O}_{16}$ and $\text{K}_2\text{Cr}_8\text{O}_{16}$, the physical properties of $\text{K}_2\text{Mn}_8\text{O}_{16}$ are not well understood yet. First of all, the concentration of K ions tends to be reduced, and the actual composition is close to $\text{K}_{1.6}\text{Mn}_8\text{O}_{16}$. [14] At 380 K, $\text{K}_{1.6}\text{Mn}_8\text{O}_{16}$ undergoes a structural phase transition from a high-temperature tetragonal phase to a low-temperature monoclinic (almost orthorhombic) $1 \times 1 \times 1$ phase. At 250 K, $\text{K}_{1.6}\text{Mn}_8\text{O}_{16}$ exhibits another phase transition to a monoclinic $1 \times 5 \times 1$ superstructure phase with five-fold periodicity along the Mn-O double chain or the Mn-O ribbon. [14] In case of $\text{K}_x\text{Mn}_8\text{O}_{16}$, the filling of K^+ ions is $(2-x)/2$, and the ratio between Mn^{3+} and Mn^{4+} is $x/8 : (8-x)/8$. Therefore, assuming that K^+ is located at neighbors of Mn^{3+} , the K^+ ion order and the $\text{Mn}^{3+}/\text{Mn}^{4+}$ charge order can collaborate only when $(2-x):x = x:(8-x)$, namely $x=1.6$.

In the present study, we focus on the origin of the phase transition at 380 K from the tetragonal phase to the low-temperature monoclinic phase without the superstructure. Since the unit cell of $\text{K}_x\text{Mn}_8\text{O}_{16}$ contains eight Mn sites, Mn $3d$ charge and orbital ordering can occur without superstructure. In particular, since the ratio between Mn^{3+} and Mn^{4+} is $1/4 : 3/4$ for $x=2$, the charge ordering at $x=2$ is expected to be compatible with the unit cell. We have examined possible charge and orbital orderings using unrestricted Hartree-Fock calculation on a hollandite-type multi-band Mn $3d$ -O $2p$ lattice model. The calculations show that the Mn^{3+} - Mn^{4+} double exchange interaction and the Mn^{3+} - Mn^{3+} and Mn^{4+} - Mn^{4+} superexchange interaction are ferromagnetic and play important roles to stabilize the charge and orbital ordering pattern which is consistent with the $1 \times 1 \times 1$ orthorhombic or monoclinic structure.

II. METHOD

We carried out unrestricted Hartree-Fock calculation for two layers of neighboring two double-chain tunnels where 32 Mn sites and 64 O sites are considered. We employ the multiband d - p model where full degeneracy of the Mn $3d$ orbitals and O $2p$ orbitals are taken into account. [15] The Hamiltonian is given by

$$\begin{aligned}
\hat{\mathcal{H}} &= \hat{\mathcal{H}}_p + \hat{\mathcal{H}}_d + \hat{\mathcal{H}}_{pd} \\
\hat{\mathcal{H}}_p &= \sum_{kl\sigma} \epsilon_k^p p_{kl\sigma}^\dagger p_{kl\sigma} + \sum_{kl'l'\sigma} V_{kl'l'}^{pp} p_{kl\sigma}^\dagger p_{kl'\sigma} + \text{h.c.} \\
\hat{\mathcal{H}}_d &= \epsilon_d^0 \sum_{i\alpha m\sigma} d_{i\alpha m\sigma}^\dagger d_{i\alpha m\sigma} + \sum_{i\alpha m m' \sigma \sigma'} h_{mm' \sigma \sigma'} d_{i\alpha m\sigma}^\dagger d_{i\alpha m' \sigma'} \\
&\quad + u \sum_{i\alpha m} d_{i\alpha m\uparrow}^\dagger d_{i\alpha m\uparrow} d_{i\alpha m\downarrow}^\dagger d_{i\alpha m\downarrow} \\
&\quad + u' \sum_{i\alpha m m'} d_{i\alpha m\uparrow}^\dagger d_{i\alpha m\uparrow} d_{i\alpha m'\downarrow}^\dagger d_{i\alpha m'\downarrow} \\
&\quad + (u' - j) \sum_{i\alpha m m' \sigma} d_{i\alpha m\sigma}^\dagger d_{i\alpha m\sigma} d_{i\alpha m' \sigma}^\dagger d_{i\alpha m' \sigma} \\
&\quad + j \sum_{i\alpha m m'} d_{i\alpha m\uparrow}^\dagger d_{i\alpha m\uparrow} d_{i\alpha m'\downarrow}^\dagger d_{i\alpha m'\downarrow} \\
&\quad + j' \sum_{i\alpha m m'} d_{i\alpha m\uparrow}^\dagger d_{i\alpha m\uparrow} d_{i\alpha m'\downarrow}^\dagger d_{i\alpha m'\downarrow} \\
\hat{\mathcal{H}}_{pd} &= \sum_{kml\sigma} V_{kml}^{pd} d_{kml\sigma}^\dagger p_{kl\sigma} + \text{h.c.}
\end{aligned}$$

Here, $d_{i\alpha m\sigma}^\dagger$ are creation operators for the Mn $3d$ electrons at site α of the i^{th} unit cell and $d_{kml\sigma}^\dagger$ and $p_{kl\sigma}^\dagger$ are creation operators for Bloch electrons which are constructed from the m^{th} component of the Mn $3d$ orbitals and from the l^{th} component of the O $2p$ orbitals, respectively, with wave vector \mathbf{k} . The matrix $h_{mm' \sigma \sigma'}$ represents the crystal field splitting. The transfer integrals between the O $2p$ orbitals $V_{kl'l'}^{pp}$ are given by Slater-Koster parameters ($pp\sigma$) and ($pp\pi$) which are fixed at 0.60 eV and -0.15 eV respectively. The transfer integrals between the Mn $3d$ and O $2p$ orbitals V_{kml}^{pd} are represented by ($pd\pi$) and ($pd\sigma$). They are fixed as ($pd\sigma$) = -2.0 eV and ($pd\pi$) = 0.9 eV. Kanamori parameters u , u' , j , and j' satisfies $u = u' + j + j'$ and $j' = j$. u and j are fixed at 7.3 eV and 0.8 eV, respectively. The O $2p$ -to-Mn $3d$ charge transfer energy is $\Delta = \epsilon^d - \epsilon^p + nU$ where $U = u - 20j/9$ and n is the number of Mn $3d$ electrons. Δ is set to 1.44 eV in the present calculation which is close to typical Δ values for Mn⁴⁺ oxides. [16]

III. RESULTS AND DISCUSSION

The unrestricted Hartree-Fock analysis for K₂Mn₈O₁₆ with the reasonable parameter set provides ferromagnetic solutions with several charge ordering patterns. The charge ordering patterns are illustrated in Fig. 1. The energies of those states are listed in Table III.

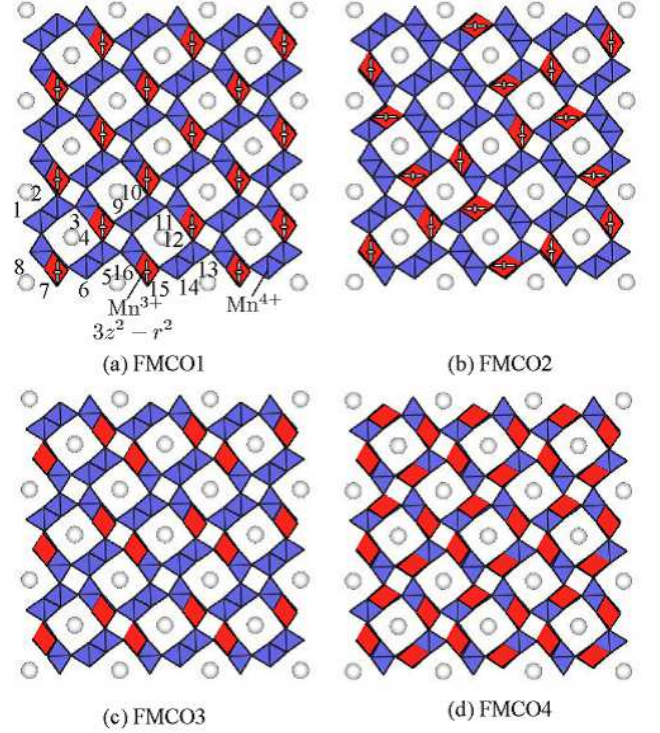


FIG. 1: (color online) Charge ordering patterns for ferromagnetic states with Mn³⁺ : Mn⁴⁺ = 1/4 : 3/4 which are labelled as (a) FMCO1, (b) FMCO2, (c) FMCO3(c), and (d) FMCO4.

TABLE I: Energy per unit cell of the FMCO2, FMCO3, and FMCO4 states relative to the most stable FMCO1 state.

State	FMCO2	FMCO3	FMCO4
Energy (eV)	0.008	0.252	0.276

The most stable state is the FMCO1 state which is shown in Fig. 1(a). Here, the charge ordering pattern in the a-b plane is illustrated. There are two kinds of double chains running along the c axis in the FMCO1 state. The one consists of only Mn⁴⁺O₆ octahedra, and the other consists of Mn³⁺O₆ and Mn⁴⁺O₆ octahedra. In the latter type of double chain, the Mn³⁺ and Mn⁴⁺ sites are aligned along the c axis in straight lines, respectively. As for the orbital ordering, at the Mn³⁺ sites with one e_g electron, the Mn $3d$ $3z^2 - r^2$ orbital [indicated by the cigar-like orbital shape in Fig. 1(a)] is directed to the corner oxygen which is sandwiched by the Mn³⁺ and Mn⁴⁺ sites. This situation is very similar to the Mn³⁺/Mn⁴⁺

TABLE II: Energy per unit cell of the AFMCO2, AFMCO3, and AFMCO4 states relative to the most stable FMCO1 state.

State	AFMCO1	AFMCO2	AFMCO3
Energy (eV)	3.045	1.448	0.965

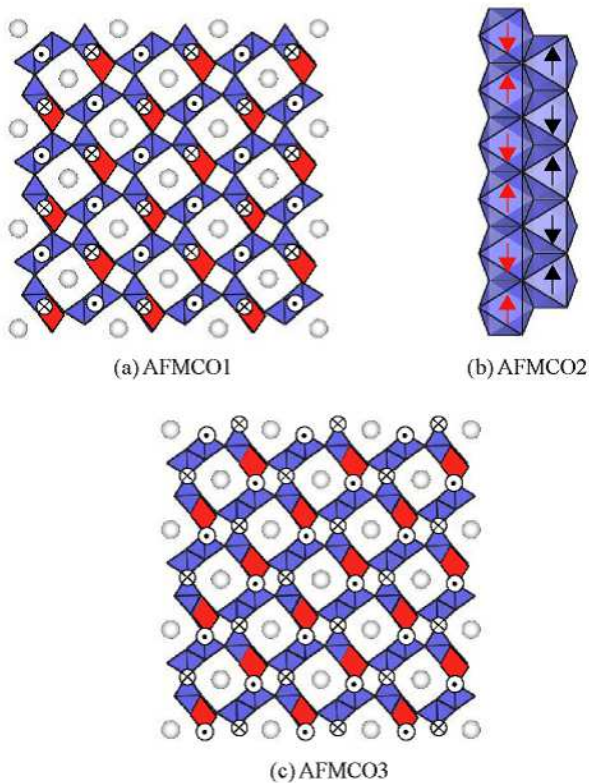


FIG. 2: (color online) Charge ordering patterns for antiferromagnetic states with $\text{Mn}^{3+} : \text{Mn}^{4+} = 1/4 : 3/4$ which are labeled as (a) AFMCO1, (b) AFMCO2, and (c) AFMCO3. The closed circles and crosses indicate the spin up and down sites, respectively.

mixed valence perovskite-type Mn oxides. [17]

Figures 1(b)-(d) show other three kinds of ferromagnetic solutions with reasonable symmetries. The FMCO2 state is similar to the FMCO1 state. The Mn^{3+} and Mn^{4+} sites are aligned along the c axis in straight lines. However, the charge ordering pattern in the a - b plane keeps the tetragonal symmetry. In the FMCO3 state, the charge ordering pattern in the a - b plane is the similar to (but somewhat different from) the FMCO1 and FMCO2 states but the Mn^{3+} and Mn^{4+} ions stack alternately along the double chains or the c axis. In the FMCO4 state, one plane has the charge ordering pattern with $\text{Mn}^{3+} : \text{Mn}^{4+} = 1/2 : 1/2$ and the next plane is filled with Mn^{4+} . These states are higher in energy than the FMCO1 state (see Table. III).

Since $\text{K}_{1.6}\text{Mn}_8\text{O}_{16}$ becomes antiferromagnetic at low temperature experimentally, we also investigated antiferromagnetic solutions of the present model calculation to elucidate the magnetic property of the system. Figure 2 shows three different types of antiferromagnetic configurations. In the AFMCO1 state, the Mn $3d$ spins are antiferromagnetic between corner-sharing octahedra as shown in Fig. 2(a). The charge-ordering pattern of the AFMCO1 state is the same as the most stable FMCO1

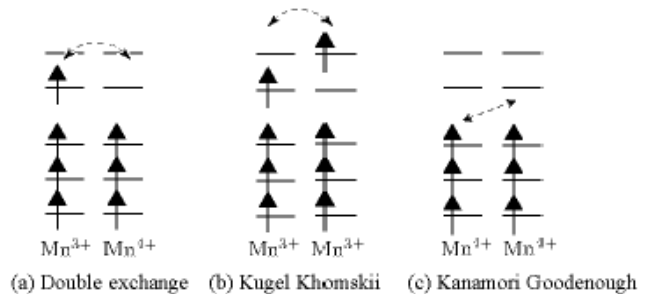


FIG. 3: Schematic pictures for (a) Mn^{3+} - Mn^{4+} double exchange interaction, (b) Mn^{3+} - Mn^{3+} Kugel-Khomskii superexchange interaction, and (c) Mn^{4+} - Mn^{4+} Goodenough-Kanamori superexchange interaction.

state, and both the FMCO1 and AFMCO state have the ferromagnetic double chains with Mn^{4+}O_6 octahedra and with Mn^{3+}O_6 and Mn^{4+}O_6 octahedra. Therefore, the energy difference between the FMCO1 and AFMCO1 states is due to the Mn^{3+} - Mn^{4+} double exchange interaction between the corner-sharing MnO_6 octahedra or between the neighboring double chains. In the AFMCO2 state, the Mn $3d$ spins are antiferromagnetic between the edge-sharing octahedra in the double chain along the c axis [see Fig. 2(b)], whereas the spin and charge arrangement in the a - b plane of the AFMCO2 is the same as the most stable FMCO1 state. In the AFMCO3 state, the Mn $3d$ spins are antiferromagnetic between the edge-sharing octahedra in the double chain along the a - b plane [see Fig. 2(c)], whereas the ferromagnetic coupling between the corner-sharing MnO_6 octahedra and that along the c -axis are the same as the most stable FMCO1 state. Compared to the ferromagnetic states, all the obtained antiferromagnetic states have much higher energy values (see Table. III). In the present calculation, antiferromagnetic coupling between far-distant-neighbors is not considered. We speculate that the antiferromagnetic state of $\text{K}_{1.6}\text{Mn}_8\text{O}_{16}$ is of helical type stabilized by nearest neighbor ferromagnetic coupling and far-distant-neighbor antiferromagnetic coupling. The AFMCO2 and AFMCO3 states are much lower in energy than the AFMCO1 state, indicating that the ferromagnetic double exchange interaction between the corner-sharing MnO_6 octahedra is much stronger than the ferromagnetic coupling between the edge-sharing octahedra.

At this stage, we discuss the origin of the spin-charge-orbital ordering of the FMCO1 state. As a reason of ferromagnetic coupling between the Mn spins, three types of electronic exchange interactions are possible for this system which are shown schematically in Fig. 3. The Mn^{3+} - Mn^{4+} ferromagnetic coupling is derived from the double exchange interaction which can be enhanced by the orbital ordering of the Mn^{3+} site. The Mn^{3+} - Mn^{3+} fer-

romagnetic coupling (along the c axis) is induced by the superexchange interaction with orbital degeneracy, which is explained by Kugel-Khomskii mechanism. As for the Mn^{4+} - Mn^{4+} superexchange interaction with the Mn-O-Mn bond in the 90° angle configuration, the ferromagnetic coupling is explained by Kanamori-Goodenough rule. Among the antiferromagnetic states, the AFMCO3 state is more stable than the AFMCO1 and AFMCO2 states, which indicates that the double exchange type ferromagnetic interaction between corner sharing MnO_6 octahedra is the strongest and the Mn^{3+} - Mn^{3+} ferromagnetic coupling along the c axis is the second strongest. The difference in the Mn^{3+} - Mn^{4+} double exchange interaction should be responsible for the small energy difference between the FMCO1 and FMCO2 states. The number of Mn $3d$ spin at each Mn site of the FMCO1 state is shown in Fig. 4(a). The 16 Mn sites in the first layer are labelled as 1-16 which is shown in Fig. 1(a). The remaining 16 Mn sites in the second layer are labelled as 17-32. The Mn^{3+} sites have $\sim 3.7 \mu_B$. Whereas most of the Mn^{4+} sites have $\sim 3.3 \mu_B$, the Mn^{4+} sites sharing the corner oxygens with the Mn^{3+} sites have $\sim 3.5 \mu_B$. The increase of the Mn $3d$ spins in the Mn^{4+} sites is due to the leakage of the Mn $3d e_g$ spins by the double exchange coupling. Since the distance between the neighboring Mn^{3+} chains is shorter in the FMCO2 state than that in the FMCO1 state, the energy gain by the double exchange interaction can be slightly larger in the FMCO1 state. In the FMCO1 state, the orbital ordering of the Mn^{3+} site contributes to enhance the double exchange interaction between the Mn^{3+} and Mn^{4+} sites. This charge-orbital ordering pattern of the FMCO1 state does not have tetragonal symmetry whereas it is compatible with the unit cell of $\text{K}_2\text{Mn}_8\text{O}_{16}$. Therefore, the FMCO1 state with $1 \times 1 \times 1$ unit cell is consistent with the intermediate phase of $\text{K}_{1.6}\text{Mn}_8\text{O}_{16}$ realized between 250 K and 380 K.

TABLE III: Hole doping dependence of band gap of the FMCO1 state for $\text{K}_{2-x}\text{Mn}_8\text{O}_{16}$.

x	0.0	0.25	0.5	0.75	1.0	1.25	1.5	1.75
Gap (eV)	0.419	0.130	0.039	0.120	0.060	0.120	0.00	0.00

In the next step, we examine the stability of the FMCO1 state against the reduction of K content or the hole doping to the Mn_8O_{16} lattice. Figure 4 and Table III show the hole doping effect on the system where the reference point is set to the FMCO1 state of $\text{K}_2\text{Mn}_8\text{O}_{16}$. The total number of the Mn $3d$ and O $2p$ electrons for $\text{K}_2\text{Mn}_8\text{O}_{16}$ is 488 in the present model, and the hole doping corresponds to reduction of K atoms from the system. The total number of the Mn $3d$ and O $2p$ electrons is $488 - x$ in the present model for $\text{K}_{2-0.25x}\text{Mn}_8\text{O}_{16}$. As shown in Fig. 4, the charge ordering pattern remains in going from $x=2$ to $x=1$, indicating that the FMCO1 state obtained for $\text{K}_2\text{Mn}_8\text{O}_{16}$ is relevant for $\text{K}_{1.6}\text{Mn}_8\text{O}_{16}$. The charge ordering pattern is slightly disturbed by the hole

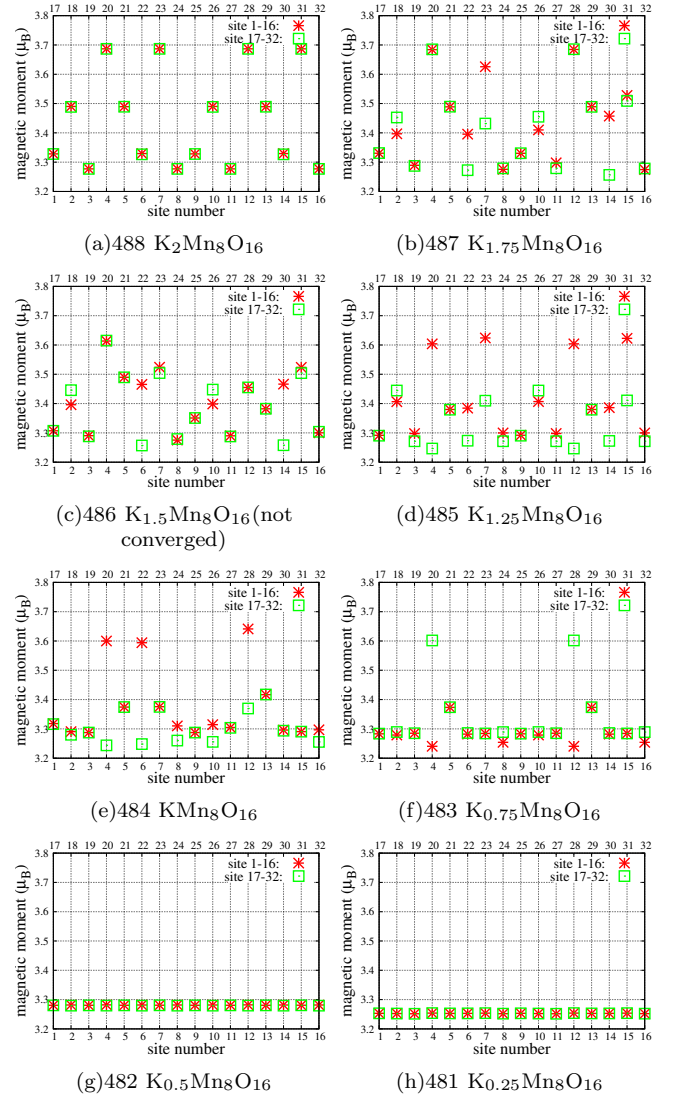


FIG. 4: (color online) Magnitudes of Mn $3d$ spins for 32 Mn sites in the FMCO1 state obtained in the present model calculation. Hole doping level x is set to (a) $x=0.0$, (b) $x=0.25$, (c) $x=0.5$, (d) $x=0.75$, (e) $x=1.0$, (f) $x=1.25$, (g) $x=1.5$, and (h) $x=1.75$.

doping which can couple with the superstructure along the c -axis due to the K vacancy ordering and would be an origin of far-distant-neighbor antiferromagnetic coupling. As shown in Table III, the magnitude of the band gap tends to decrease as the amount of hole increases until the transition to a metallic state at $\text{K}_{0.5}\text{Mn}_8\text{O}_{16}$. It should be noted that in the states $\text{K}_{1.75}\text{Mn}_8\text{O}_{16}$, $\text{K}_{1.25}\text{Mn}_8\text{O}_{16}$, and $\text{KMn}_8\text{O}_{16}$, the Mn $3d e_g$ level is partially occupied at the "Mn $^{4+}$ " sites sharing the corner oxygens with the Mn^{3+} sites and, these states have relatively wide gaps, which we infer results from the double exchange interaction between Mn^{3+} and Mn^{4+} .

IV. CONCLUSION

In conclusion, we investigate spin-charge-orbital ordering in a $\text{Mn}^{3+}/\text{Mn}^{4+}$ mixed valence state on a hollandite-type lattice using unrestricted Hartree-Fock calculation on a multi-band Mn $3d$ -O $2p$ lattice model. The Mn^{3+} - Mn^{4+} ferromagnetic coupling due to the double exchange interaction plays essential role to stabilize the charge ordering pattern. In addition, The Mn^{3+} - Mn^{3+} and Mn^{4+} - Mn^{4+} ferromagnetic couplings along the c axis is induced by the Kugel-Khomskii and Kanamori-Goodenough mechanisms. The most stable

charge and orbital ordering pattern is consistent with the $1 \times 1 \times 1$ orthorhombic or monoclinic structure realized in $\text{K}_{1.6}\text{Mn}_8\text{O}_{16}$.

Acknowledgement

The authors would like to thank Prof. Y. Ueda, Dr. M. Isobe, and Prof. D. I. Khomskii for valuable discussions. M. F. is supported by Japan Society for the Promotion of Science through Program for Leading Graduate Schools (MERIT).

-
- [1] N. F. Mott, *Metal-Insulator Transitions*, (Taylor & Francis, London, 1990).
 - [2] N. Tsuda, K. Nasu, A. Fujimori, and K. Shiratori, *Electronic Conduction in Oxides*, (Springer-Verlag, Berlin, 2000).
 - [3] M. Imada, A. Fujimori, and Y. Tokura, *Rev. Mod. Phys.* **70**, 1039 (1998).
 - [4] E. J. W. Verwey, *Nature(London)* **144**, 327 (1939).
 - [5] S. Kachi, K. Kosuge, and H. Okinaka, *J. Solid State Chem.* **6**, 258 (1973).
 - [6] M. Isobe, S. Koishi, N. Kouno, J. Yamaura, T. Yamauchi, H. Ueda, H. Gotou, T. Yagi, and Y. Ueda, *J. Phys. Soc. Jpn.* **75**, 073801 (2006).
 - [7] K. Hasegawa, M. Isobe, T. Yamauchi, H. Ueda, J. I. Yamaura, H. Gotou, T. Yagi, H. Sato, and Y. Ueda, *Phys. Rev. Lett.* **103**, 146403 (2009).
 - [8] S. Horiuchi, T. Shirakawa, and Y. Ohta *Phys. Rev. B* **77**, 155120 (2008).
 - [9] M. Sakamaki, T. Konishi, and Y. Ohta, *Phys. Rev. B* **80**, 024416 (2009).
 - [10] P. Mahadevan, A. Kumar, D. Choudhury, and D. D. Sarma, *Phys. Rev. Lett.* **104**, 256401 (2010).
 - [11] A. C. Komarek, M. Isobe, J. Hemberger, D. Meier, T. Lorenz, D. Trots, A. Cervellino, M. T. Fernández-Díaz, Y. Ueda, and M. Braden, *Phys. Rev. Lett.* **107**, 027201 (2011).
 - [12] J. van den Brink and D. I. Khomskii, *J. Phys.: Condens. Matter* **20**, 434217 (2008).
 - [13] T. Toriyama, A. Nakao, Y. Yamaki, H. Nakao, Y. Murakami, K. Hasegawa, M. Isobe, Y. Ueda, A. V. Ushakov, D. I. Khomskii, S. V. Streltsov, T. Konishi, and Y. Ohta, *Phys. Rev. Lett.* **107**, 266402 (2011).
 - [14] T. Kuwabara, M. Isobe, H. Gotou, T. Yagi, D. Nishio-Hamane, and Y. Ueda, *J. Phys. Soc. Jpn.* **81**, 104701 (2012).
 - [15] T. Mizokawa and A. Fujimori, *Phys. Rev. B* **54**, 5368 (1996).
 - [16] H. Wadati, D. G. Hawthorn, T. Z. Regier, G. Chen, T. Hitosugi, T. Mizokawa, A. Tanaka, and G. A. Sawatzky *Appl. Phys. Lett.* **97**, 022106 (2010).
 - [17] T. Mizokawa and A. Fujimori, *Phys. Rev. B* **56**, 493 (1997).